SCGB1A1 as a novel biomarker and promising therapeutic target for the management of HNSCC

JING WANG[1,2*], QIANQIAN XU[3*], JIANGBO YU[1], AOTIAN XU[4], LIZHENG YU[5], ZHENGGANG CHEN[1], YANG CAO[1], RONGTAO YUAN[1] and ZHONGJIE YU[4]

[1]Center of Oral Medicine, Qingdao Municipal Hospital, Qingdao, Shandong 266000, P.R. China; [2]R&D, Shandong Yinfeng Life Science Research Institute, Jinan, Shandong 250000, P.R. China; [3]Qingdao Cancer Institute, School of Basic Medicine, Qingdao Medical College, Qingdao University, Qingdao, Shandong 266000, P.R. China; [4]R&D, Qingdao Sino-cell Biomedicine Co., Ltd., Qingdao, Shandong 266000, P.R. China; [5]Department of Vascular Surgery, Qingdao Medical College, Qingdao University, Qingdao, Shandong 266000, P.R. China

Received February 22, 2024; Accepted July 18, 2024

DOI: 10.3892/ol.2024.14660

Abstract. Head and neck cancer (HNC) is the sixth most common type of cancer worldwide, and head and neck squamous cell carcinoma (HNSCC) accounts for 90% of HNC cases. Furthermore, HNSCC accounts for 400,000 cancer-associated deaths worldwide each year. However, at present there is an absence of a versatile biomarker that can be used for diagnosis, prognosis evaluation and as a therapeutic target for HNSCC. In the present study, bioinformatics analysis was used to assess the relationship between hub genes and the clinical features of patients with HNSCC. The findings from the bioinformatics analysis were then verified using clinical samples and *in vitro* experiments. A total of 51 overlapping genes were identified from the intersection of differentially expressed genes and co-expressed genes. The top 10 hub genes were obtained from a protein-protein interaction network of overlapping genes. Among the hub genes, only secretoglobin family 1A member 1 (*SCGB1A1*) was significantly associated with both overall and disease-free survival. Specifically, upregulated *SCGB1A1* expression levels were associated with prolonged overall and disease-free survival. Moreover, the *SCGB1A1* expression levels were negatively correlated with drug sensitivity. Notably, it was demonstrated that SCGB1A1 was involved in tumor immunoreaction by affecting the infiltration of cells and checkpoint regulation of immune cells. Additionally, it was shown that SCGB1A1 regulated multiple key cancer-related signaling pathways, including extracellular matrix receptor interaction, transforming growth factor-β and tumor metabolism signaling pathways. Based on the results of the present study, *SCGB1A1* may serve as a novel biomarker for predicting the diagnosis, prognosis and therapeutic effectiveness of certain drugs in patients with HNSCC. Moreover, SCGB1A1 may serve as a potential therapeutic target for the management of HNSCC.

Correspondence to: Dr Rongtao Yuan, Center of Oral Medicine, Qingdao Municipal Hospital, 5 Donghai Middle Road, Qingdao, Shandong 266000, P.R. China
E-mail: yuanrongtao@163.com

Dr Zhongjie Yu, R&D, Qingdao Sino-cell Biomedicine Co., Ltd., Baishahe Medical and Health Industrial Park, 108 Yihai Road, Chengyang, Qingdao, Shandong 266000, P.R. China
E-mail: zhongjiework@163.com

*Contributed equally

Abbreviations: HNC, head and neck cancer; HNSC/HNSCC, head and neck squamous cell carcinoma; DEG, differentially expressed gene; GEO, Gene Expression Omnibus; WGCNA, weighted gene co-expression network analysis; GO, Gene Ontology; KEGG, Kyoto Encyclopedia of Genes and Genomes; PPI, protein-protein interaction; GSEA, Gene Set Enrichment Analysis; RT-qPCR, reverse transcription-quantitative PCR; SCGB1A1, secretoglobin family 1A member 1

Key words: bioinformatics analysis, head and neck squamous cell carcinoma, SCGB1A1, tumor immunology, tumor metabolism

Introduction

Head and neck cancer (HNC) is the sixth most common type of cancer (1), accounting for 2.8% of all malignant cancer cases worldwide (2). HNC is a significant cause of morbidity and mortality across the globe, with 890,000 new cases reported in 2020 (3) and >400,000 deaths predicted annually worldwide (4). Head and neck squamous cell carcinoma (HNSCC) accounts for 90% of HNC cases and describes a group of heterogeneous cancers that emerge from the upper aerodigestive tract that affect the oral and nasal cavity, salivary glands, oropharynx, pharynx, larynx, paranasal sinuses, local lymph nodes and even the middle ear (5-7). HNSCC is a complex disease characterized by alterations in multiple genes and pathways (5,8). However, the underlying molecular mechanisms of its development and prognosis require further investigation. Identifying novel therapeutic targets and prognostic biomarkers of HNSCC will contribute to a deeper understanding of HNSCC and may assist in prolonging the survival and improving the quality of life of patients.

With the development of high-throughput sequencing technologies, using mRNA-sequencing (seq) to identify HNSCC-related genes and pathways has emerged as a valuable

method for cancer research (9). Numerous mRNA datasets have been produced for studying a myriad of biological challenges. These datasets facilitate extensive gene analysis efforts. For instance, the *TP53* gene is frequently mutated in patients with HNSCC, as evidenced by numerous studies (10-12). In *TP53*-mutated HNSCC, sestrin 1, UHRF1BP1 and microRNA-377-3p have been identified as prognostic markers (13). Furthermore, CD3D serves as an independent and favorable prognostic marker for immunotherapy in patients with HNSCC (14). The currently identified biomarkers for HNSCC have limited utility, primarily confined to patient prognosis analysis, thereby underscoring the imperative need for a comprehensive and versatile biomarker in this specific context.

In the present study, overlapping genes were identified by integrating differentially expressed genes (DEGs) and co-expressed genes using data obtained from The Cancer Genome Atlas (TCGA) and Gene Expression Omnibus (GEO). A total of 51 overlapping genes were analyzed using systematic bioinformatics to explore the underlying molecular mechanisms of HNSCC pathogenesis and to identify a novel biomarker and a candidate therapeutic target for HNSCC. Additionally, immune analysis was performed on the selected targets to further predict the therapeutic value of immunotherapy. The present study investigated and validated a novel, comprehensive tumor biomarker termed secretoglobin family 1A member 1 (*SCGB1A1*), which exhibits significant potential for the diagnosis, evaluation of treatment efficacy and analysis of patient prognosis in HNSCC. Furthermore, the present study investigated whether SCGB1A1 plays a pivotal role in the metabolic and immune regulatory processes within HNSCC, thereby emerging as a promising therapeutic target for effective management of HNSCC.

Materials and methods

Data collection. After conducting a comprehensive search of the GEO database (https://www.ncbi.nlm.nih.gov/geo/) for HNSCC as well as normal head and neck tissues, the available datasets were narrowed down to 40 datasets based on specific criteria, such as array-based expression profiling and human tissue type. The GSE30784 dataset (15,16) was selected for data analysis based on the sample size (the other available datasets included fewer samples), aiming to obtain more precise data. This dataset consists of 45 normal tissues and 167 HNSCC tissues. The GPL570 platform (Affymetrix; Thermo Fisher Scientific, Inc.; version 1.38.0) was used to analyze the microarray data. For this, after downloading the GEO dataset, the gene expression matrix was extracted and the merge function was utilized to convert probe names into corresponding gene names. Finally, 20,549 genes were selected for subsequent analysis (17). In addition, relevant datasets and clinical information on HNSCC were also obtained from TCGA (18) (dataset: TCGA-HNSC; https://portal.gdc.cancer.gov). A total of 83 samples (13 normal samples and 70 cancer samples) and 14,212 genes were selected for subsequent analysis.

Identification of DEGs. DEG analysis was performed as described in our previous study with some modifications (19). Briefly, the 'limma' package in R (version; 4.0.3) was used to analyze the data obtained from TCGA and the GEO (20,21). During the gene differential analysis process, a logarithmic transformation was applied to the data in the GeneMatrix file to normalize its overall scale. The Log2FoldChange (FC) values ranged between 0 and 2, with only 2 genes exhibiting absolute values >1. To ensure suitability for subsequent analyses, the range of absolute FC values was expanded to include those as low as 0.2. Therefore, the DEGs between adjacent normal tissues and HNSCC samples were defined based on a |logFC|>1 and false discover rate (FDR)<0.05 for the data obtained from TCGA, or |logFC|>0.2 (22) and FDR<0.05 for data obtained from the GEO. Next, the DEGs in the datasets were output in the form of a volcano plot using the 'ggplot' package in R (23).

Weighted gene co-expression network analysis (WGCNA). The 'WGCNA' package in R was used to construct the weighted gene co-expression network and to classify the co-expression modules (24,25). First, gene correlations and an adjacency matrix were calculated. Next, this matrix was transformed into a topological overlap matrix (TOM) to reduce noise and false correlations [gene co-expression matrix, S=(Sij); adjacency function, Aij=power (Sij, β)=| Sij| β) |GS| >0.5, |MM| >0.8]. TOM was used to convert the correlation between genes into a distance matrix. The distance matrix was used for cluster analysis, and the genes were classified into the same module. Finally, the significant modules associated with traits were determined and selected for subsequent analysis (24,26).

Unsupervised clustering analysis. To identify genes that were significantly differentially expressed in HNSCC in the data obtained from TCGA, unsupervised clustering analysis was performed using 'ConsensusClusterPlus' in R (27).

Screening of overlapping genes by the intersection of differential genes and differential modules. The overlapping genes between the DEGs were screened using the limma package, and the co-expression genes of modules were screened by differential clinical characteristics. A Venn diagram was constructed using the 'VennDiagram' package in R (28).

Gene Set Enrichment Analysis (GSEA). Gene Ontology (GO) and Kyoto Encyclopedia of Genes and Genomes (KEGG) analyses and GSEA were performed as described in our previous study with slight modifications (19). The R packages 'clusterProfiler', 'ggplot2', 'enrichplot' and 'org.Hs.eg.db' were used to perform the GO and KEGG pathway analyses (29,30). P- and Q-values <0.05 were considered significantly enriched. GSEA of the hub genes in the high-expression group [samples exhibiting expression levels surpassing the median expression level of the target gene (SCGB1A1) in the expression matrix were categorized as belonging to the high-expression group] was performed using the KEGG gene sets and the hallmarks from the Molecular Signatures Database (MSigDB; version 7.5.1) gene sets were used to identify the enriched pathways (31). Each enrichment analysis was performed using 1,000x gene set permutations. Pathways with an FDR<0.05 and a nominal P<0.05 were considered significantly enriched.

Protein-protein interaction (PPI) network construction. The PPI network was constructed as described in our previous study with slight modifications (19). Briefly, the PPIs of the identified DEGs were predicted using the Search Tool for the Retrieval of Interacting Genes/Proteins (STRING), an online tool for determining the interacting genes/proteins (https://cn.string-db.org/) (32). Then, the intersecting genes were identified from the PPI network. The Cytoscape (version 3.7.2) platform was utilized to visualize the interactive network of overlapping genes, and a confidence level of >0.95 was used to build the network (33,34).

Survival analysis of the hub genes. Survival analysis of the hub genes was performed as described previously with slight modifications (19). The R packages 'survival' and 'survminer' were used to analyze the clinical information of the hub genes; 'survival' was used for Kaplan-Meier survival curve analysis and 'survminer' was used for 'ggsurvplot' visualization and statistical analysis (all using the default settings) (35,36). $P<0.05$ was considered to indicate a statistically significant difference.

Pan-cancer analysis. RNA-sequencing expression profiles and corresponding clinical information for pan-cancer were downloaded from TCGA (https://portal.gdc.com). All the analysis methods were implemented by R version 4.0.3. If not stated otherwise, two-group data comparisons were performed by the Wilcoxon test. $P<0.05$ were considered to indicate a statistically significant difference (https://www.aclbi.com/static/index.html#/pan_cancer).

Clinical samples. Clinical samples were collected according to a protocol approved by the Ethics Committee of the Medical College of Qingdao University (Qingdao, China; approval no. QDU-HEC-2022166). All patients consented to participation in the present study, signed informed consent forms and agreed to the publication of the collected data. The patient inclusion criteria were as follows: Patients with HNSCC without any other diseases, including chronic diseases. From March, 2023 to September, 2023, a total of 12 oral squamous cell carcinoma tissue samples (from 7 male and 5 female patients; median age, 58 years old; age range, 38-79 years old) were collected during surgery at the Qingdao Municipal Hospital. Adjacent normal tissues were also collected from the same patients.

Cell culture and treatment. CAL27 and SCC-9 cells (both from Hunan Fenghui Biotechnology Co., Ltd.) were cultured in DMEM-H and DMEM-H/F12 (both from Gibco; Thermo Fisher Scientific, Inc.), respectively, supplemented with 10% FBS (TransGen Biotech Co., Ltd.) in a humidified incubator supplied with 5% CO_2 air at 37˚C. Cells were treated with 0, 1 or 3 μM doxorubicin (DOX; Selleck Chemicals) in medium for 12 h.

Lentiviral (Lv) vector. The Lv-SCGB1A1 overexpression vector was constructed in our laboratory. The *SCGB1A1* sequence was downloaded from the NCBI (https://www.ncbi.nlm.nih.gov/gene/7356), and the primers for *SCGB1A1* were designed using SnapGene 4.0 (https://www.snapgene.com/). The primer sequences were as follows: Forward 5'-ATGAAACTCGCTGTCACCCTCACC-3' and reverse 5'-CTAATTACACAGTGAGCTTTGGGCTATTTTTTCC-3'. The amplified products were then inserted into the PCDH vector (Hunan Fenghui Biotechnology Co., Ltd.) and used to establish a stably expressing cell line. The negative control (LV-control) was an empty plasmid that did not express SCGB1A1. The 2nd generation system (Hunan Fenghui Biotechnology Co., Ltd.) was used to producing lentivirus. For this, 80% confluent 293T cells (Hunan Fenghui Biotechnology Co., Ltd.) in a 10-cm dish were transfected with 10 μg SCGB1A1 or control plasmid, 5 μg PMD2G plasmid and 5 μg PsPAX2 plasmid using Lipofectamine 3000 Transfection Reagent (Invitrogen; Thermo Fisher Scientific, Inc.), according to the manufacturer's instructions. The cells were incubated in a humidified incubator supplied with 5% CO_2 air at 37˚C. After 6 h, the transfection medium was replaced with DMEM-H containing 5% FBS and cultured for another 48 h for the generation of lentivirus. The lentiviral particles were collected using Amicon® Ultra-15 (Merck KGaA). CAL27 cells were transduced with SCGB1A1 or control lentivirus at MOI=10 and the transduction medium contained 1% lentiBOOST (Sirion Biotech GmbH) to promote viral transduction. After 18 h, the transduction medium was replaced with normal medium. After another 72 h, 4 μg/ml puromycin (Selleck Chemicals) was used for selection and maintenance of the stable cell line. The stable cell line was used for subsequent experiments 1 week later.

To investigate the influence of *SCGB1A1* overexpression on cell viability, $2x10^4$ cells/well were seeded into 96-well plates and the cell viability was detected by Cell Counting Kit-8 (CCK-8) assay once a day, continuously for 6 days. The CCK-8 assay (Dalian Meilun Biology Technology Co., Ltd.; cat. no. MA0218) was performed according to the manufacturer's protocol.

Immunohistochemistry. Paraffin-embedded sections of oral squamous cell carcinoma tissues and normal tissues were collected for immunohistochemical staining. Immunochemical staining was performed as described in our previous study (37). Briefly, tissues were fixed in 4% paraformaldehyde at 4˚C for 24 h, followed by embedding in paraffin. The tissues were cut into 5 μm sections and used for subsequent experiments. The sections were blocked with goat serum (Solarbio; cat. no. SL038) at room temperature for 1 h, then 1X endogenous peroxidase blocking buffer (Beyotime Institute of Biotechnology; cat. no. P0100B) was used to block endogenous peroxidase/phosphatase activity. Samples were incubated with a primary antibody against SCGB1A1 (1:100; Affinity Biosciences; cat. no. DF6581) at 4˚C overnight, followed by the secondary antibody [Goat Anti-Rabbit IgG (H+L) HRP; 1:200; Affinity Biosciences; cat. no. S0001] at room temperature for 1 h. Finally, the samples were incubated with DAB at room temperature for 10 min. Images were obtained using an OLYMPUS CKX53 in light mode. Figure analysis was performed using ImageJ 1.51 (National Institutes of Health).

CCK-8 assay. A total of $2x10^4$ cells/well were seeded into 96-well plates and incubated overnight for adherence. The cells were subsequently treated with 0, 1 or 3 μM DOX for

12 h. After treatment, a CCK-8 assay was performed according to the manufacturer's protocol.

Reverse transcription-quantitative PCR (RT-qPCR). RT-qPCR was used for the detection of hub gene expression as described previously (38). Total RNA was extracted from clinical samples and treated cells using an RNA isolation kit (Tiangen Biotech Co., Ltd.). RT to generate cDNA was performed using the TransScript II One-Step gDNA Removal and cDNA Synthesis SuperMix (TransGen Biotech Co., Ltd.) according to the manufacturer's instructions. TransStart Green qPCR SuperMix (TransGen Biotech Co., Ltd.) was used for qPCR. The thermocycler conditions were as follows: 94˚C for 10 min, then 94˚C for 5 sec and 60˚C for 30 sec for 40 cycles. The expression levels of the hub genes were normalized to that of β-actin and calculated using the $2^{-\Delta\Delta Cq}$ method (38). The sequences of the primers used for amplification are listed in Table SI.

Western blotting. The treated cells were lysed in RIPA lysis buffer (Shanghai Epizyme Biotech Co., Ltd.; cat. no. PC102) containing 1% protease inhibitor (Shanghai Epizyme Biotech Co., Ltd.; cat. no. GRF101). The protein concentrations were then determined using a BCA kit (Shanghai Epizyme Biotech Co., Ltd.; cat. no. ZJ101). Equal amounts of protein (20 μg) per lane were loaded and separated on a 12.5% SDS-PAGE gel, then proteins were transferred onto a PVDF membrane, which was blocked in 5% skim milk (Shanghai Epizyme Biotech Co., Ltd.; cat. no. PS112) dissolved in 1% tris-buffered saline Tween-20 (TBST) (Shanghai Epizyme Biotech Co., Ltd.; cat. no. TF103) at room temperature for 1 h with slight shaking. The membranes were next incubated with the primary SCGB1A1 (1:2,000; Rabbit; Affinity Biosciences; cat. no. DF6581) and actin (1:10,000; Rabbit; Affinity Biosciences; cat. no. AF7018) antibodies overnight at 4˚C. After washing three times with 1% TBST, the membranes were incubated with secondary antibody [Goat Anti-Rabbit IgG (H+L) HRP; 1:10,000; Affinity Biosciences; cat. no. S0001] for 1 h at room temperature. After washing three times with 1% TBST, the blots were visualized using Omni-ECL™ (Shanghai Epizyme Biotech Co., Ltd.; cat. no. SQ201). Images were obtained using an integrated chemiluminescence imaging system (Shanghai Epizyme Biotech Co., Ltd.; cat. no. XF101). Semi-quantitative analysis was performed using ImageJ 1.51 (National Institutes of Health).

Drug sensitivity and molecular docking analysis. RNA-seq expression data from HNSCC samples were downloaded from TCGA as aforementioned (https://portal.gdc.com). pRRophetic was used to predict the response of SCGB1A1 to drugs in the Cancer Genome Project database (ftp://ftp.sanger.ac.uk/pub4/cancerrxgene/releases), based on expression levels of SCGB1A1, the IC_{50} values of different drugs between SCGB1A1 high and low groups were compared using the Wilcoxon rank-sum test (39,40). The 2D structures of drugs were downloaded from PubChem (https://pubchem.ncbi.nlm.nih.gov/), transformed into 3D structures and optimized using Chem3D (https://library.bath.ac.uk/chemistry-software/chem3d). Non-polar hydrogens were added to the 3D structures using AutoDockTools (ADT; version 1.5.6; https://autodocksuite.scripps.edu/adt/) (41). The 3D structure of SCGB1A1 was downloaded from the RCSB Protein Data Bank (https://www.rcsb.org/; accession no. 7vf3) (42). The water molecules and molecular ligands were removed in ADT and non-polar hydrogens were added. AutoDock Vina (version 1.1.2) was used to simulate the docking of the drugs with the SCGB1A1 protein, and the docking conformations were visualized using PyMOL (version 2.3; Schrodinger, LLC) (43).

Immunological analysis. Immunological analysis was performed online according to the included instructions (https://www.home-for-researchers.com/static/index.html#/). RNA-seq expression profiles and the corresponding clinical information for HNSCC were downloaded from TCGA as aforementioned. The R package 'ggalluvial' was used to build the Sankey diagram. All the analytical methods and R packages were implemented by R (foundation for statistical computing 2020) version 4.0.3 (44). To assess the reliability of the results of the immune score evaluation, 'immuneeconv' was used, an R software package that integrates six of the latest algorithms, including TIMER, xCell, MCP-counter, CIBERSORT, EPIC and quanTIseq (45-48). *SIGLEC15*, *IDO1*, *CD274*, *HAVCR2*, *PDCD1*, *CTLA4*, *LAG3* and PDCD1LG2 are the transcripts associated with immune checkpoint-related genes, thus the expression of these 8 genes was assessed (44,49-52). Results derived from normal and cancer tissues were compared using the Wilcoxon test.

GeneMANIA analysis. GeneMANIA analysis was performed using the URL: http://genemania.org, application version: 3.6.0. The analyses are conducted based on the descriptions provided by others, following the default conditions (53).

Gene mutation analysis. Mutation analysis of glycolysis-related genes and cluster analysis of DEGs was performed using the somatic mutation data from TCGA. The 'maftools' function in R was used for mutation analysis, while organizing and visualizing the results using different functional packages (54).

Statistical analysis. Data are presented as the mean ± SD of at least three independent experiments. Differences between multiple groups were compared using one-way ANOVA followed by Tukey's post hoc test. The comparison of only two groups was conducted using paired t-test. The cell viability curve data were analyzed using an un-paired t-test. All statistical analyses were performed using GraphPad Prism version 5.0 (Dotmatics). $P<0.05$ was considered to indicate a statistically significant difference.

Results

The aim of the present study was to identify a potential biomarker and a candidate therapeutic target for HNSCC. The workflow of the present study is shown in Fig. 1.

DEG identification, WGCNA and cluster analysis. The GEO (20,549 genes; Table SII) and TCGA (14,212 genes; Table SIII) HNSCC datasets were used to identify DEGs. The DEGs identified from TCGA (2,479 genes) or GEO (841 genes) datasets are shown in Fig. 2A and Table SIV or Fig. S1A and Table SV,

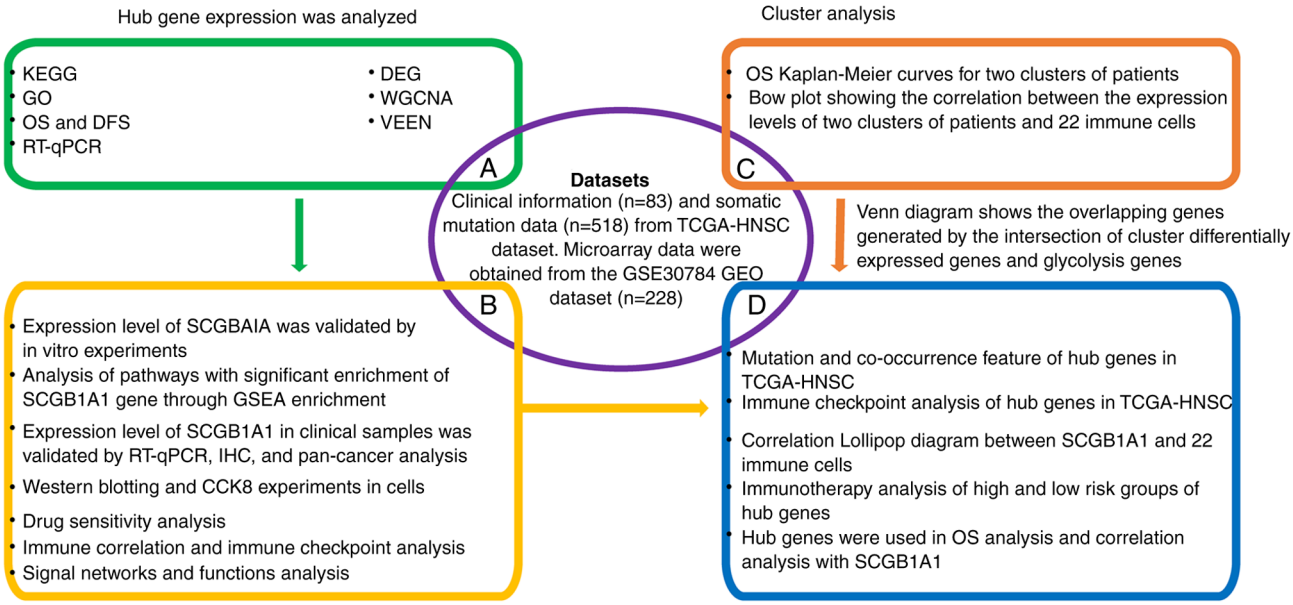

Figure 1. Workflow of the present study. KEGG, Kyoto Encyclopedia of Genes and Genomes; GO, Gene Ontology; OS, overall survival; DFS, disease-free survival; RT-qPCR, reverse transcription-quantitative PCR; DEG, differentially expressed gene; WGCNA, weighted gene co-expression network analysis; HNSC, head and neck squamous cell carcinoma; TCGA, The Cancer Genome Atlas; GEO, Gene Expression Omnibus; GSEA, Gene Set Enrichment Analysis; IHC, immunohistochemistry; CCK8, Cell Counting Kit 8; SCGB1A1, secretoglobin family 1A member 1.

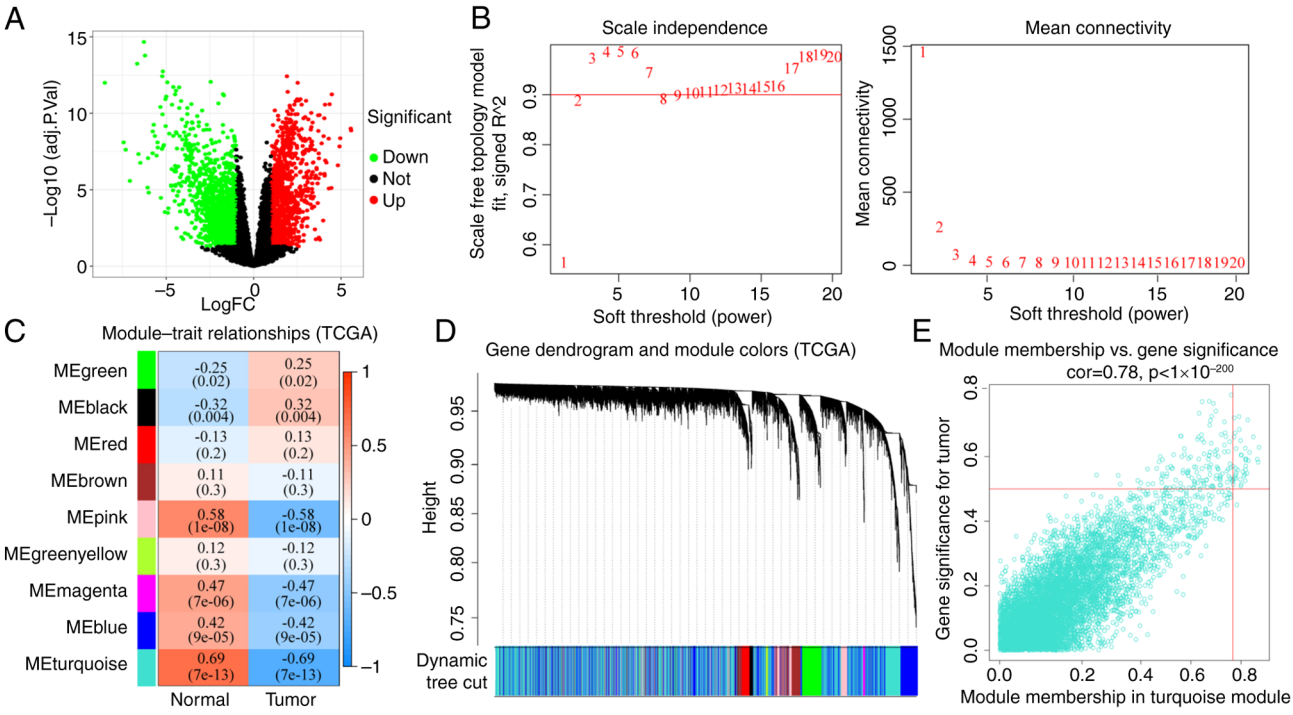

Figure 2. Analysis of DEGs and WGCNA of the data obtained from TCGA. (A) Volcano plot of the data obtained from TCGA. (B) WGCNA power selection. (C) Dendrogram of the WGCNA modules. (D) Relationship between the co-expression modules and external traits. (E) Scatter plot of module membership and gene significance for cancer in the turquoise module. DEG, differentially expressed gene; WGCNA, weighted gene co-expression network analysis; TCGA, The Cancer Genome Atlas.

respectively. The DEGs that were significantly differentially expressed between normal and tumor tissues, along with DEG expression profiles in 70 (TCGA) and 184 (GEO) patients with HNSCC, were included in the construction of a co-expression network with 9 (TCGA) and 13 (GEO) genes as the soft thresholding power β (Figs. 2B and S1B). A total of four WGCNA modules were identified (Figs. 2C and S1C). The relationships between the DEGs and the four co-expression modules were explored in Figs. S1D and 2D. The results showed that the DEGs were most commonly associated with the designated turquoise and red modules. The association between module membership and gene significance for a tumor in the turquoise

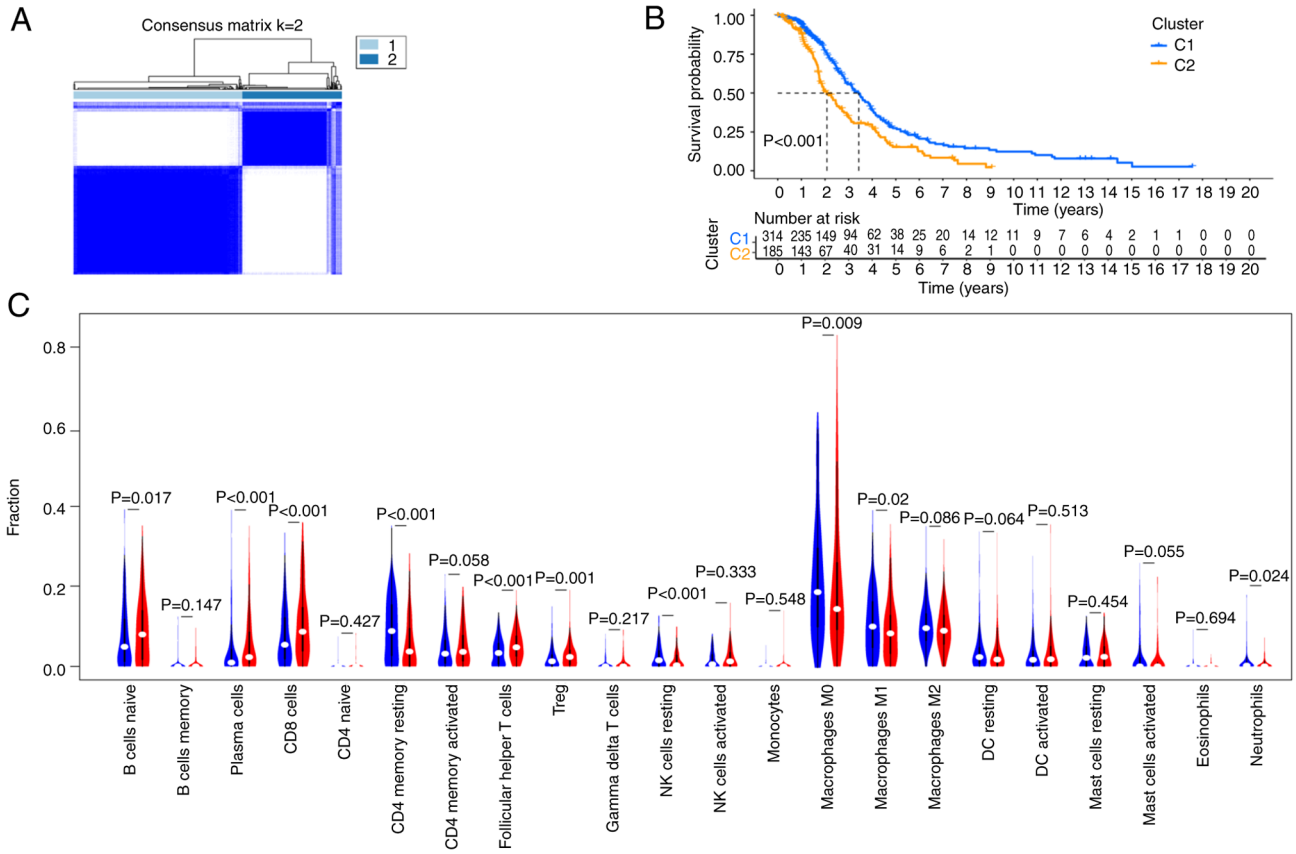

Figure 3. TCGA data clustering and immune cell characterization. (A) Unsupervised clustering analysis of TCGA-HNSC. (B) Survival analysis of patients using unsupervised cluster analysis. (C) Unsupervised cluster analysis of the differences in the levels of 22 types of immune cells between the two clusters. Cluster 1 is shown in blue and cluster 2 is shown in red. TCGA, The Cancer Genome Atlas; HNSC, head and neck squamous cell carcinoma.

and red modules was then analyzed (Figs. S2E and S1E and Tables SVI and SVII), which showed that gene significance for a tumor in the DEGs was significantly associated with the corresponding module membership. Using TCGA-HNSC dataset for unsupervised clustering analysis, the data were divided into two categories: Clusters 1 and 2 (Fig. 3A), and there was a significant difference in the median survival between these two clusters (Fig. 3B). To understand the relationship between these two clusters in immune cell infiltration, the CIBERSORT algorithm was used to study the infiltration of 22 types of immune cells. The results demonstrated that the differential genes in Clusters 1 and 2 had different immune infiltration scores for different immune cells. The proportions of Naïve B cells, plasma cells, $CD8^+$ T cells, T follicular helper cells and regulatory T cells in Cluster 2 were higher than that in Cluster 1, while the proportions of resting $CD4^+$ memory T cells, resting natural killer cells, M0 and M1 macrophages and neutrophils in Cluster 1 were higher (Fig. 3C).

Functional enrichment analysis. A total of 51 overlapping genes were identified by integrating DEGs and co-expressed genes from TCGA and GEO datasets (Fig. 4A). GO functional enrichment analysis showed that the overlapping genes were involved in the biological processes of 'ossification', 'regulation of inflammatory response' and 'regulation of sodium ion transmembrane transporter activity', the cellular components of 'coated vesicle', 'bicellular tight junction' and 'tight junction' and the molecular functions of 'retinol dehydrogenase activity', 'steroid hormone receptor activity' and 'phosphatidylserine binding' (Fig. 4B). KEGG pathway analysis indicated that the overlapping genes were involved in the 'Lysosome', 'Tight junction', 'Pathogenic Escherichia coli infection', 'Retinol metabolism', 'Rheumatoid arthritis' and 'Leukocyte transendothelial migration' pathways (Fig. 4C).

Survival analysis and expression characteristics of SCGB1A1. A PPI network was constructed using the STRING database with 72 edges and 51 nodes (Fig. S2A and B). CytoHubba was used to filter the hub genes in the PPI network. The top 10 hub genes were *CLDN8*, *CAB39L*, *PLP1*, *GPX3*, *ATP6V0A4*, *GPD1L*, cathepsin C (*CTSC*), *SCGB1A1*, ATP binding cassette subfamily A member 8 (*ABCA8*) and *SLC26A2* (Fig. S2C).

Kaplan-Meier curves were used for survival analysis, and the results revealed that *ABCA8* and *SCGB1A1* were significantly associated with overall survival (Figs. 5A, B and S3). Patients with upregulated expression levels of *ABCA8* and *SCGB1A1* had a longer overall survival time. In addition, *CTSC* and *SCGB1A1* were significantly associated with disease-free survival (Figs. 5C, D and S4). Patients with a low expression level of *CTSC* and a high expression level of *SCGB1A1* had a longer disease-free survival time. Further analysis showed that the expression levels of *SCGB1A1* were also associated with the pathological TNM stage and grade of patients with HNSCC (Fig. S5A and B). In summary, the expression level of *SCGB1A1* could be used to evaluate the prognosis of patients with HNSCC.

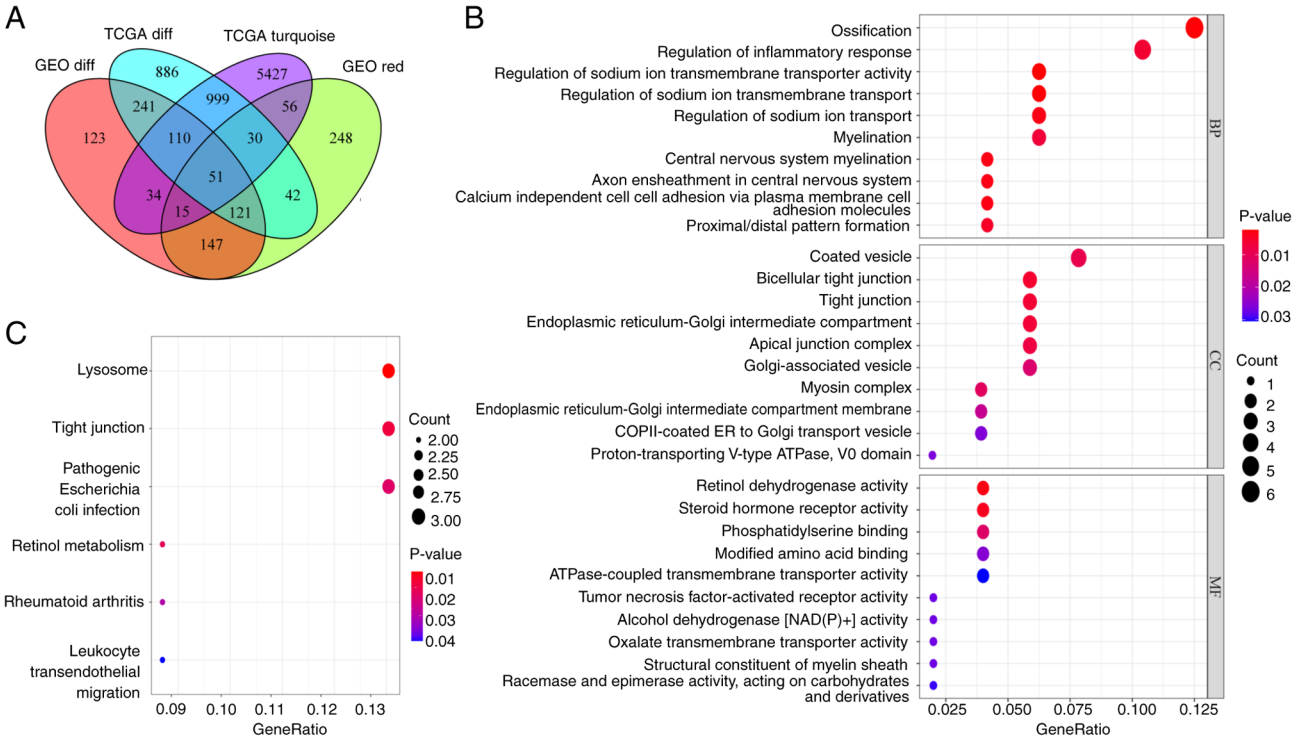

Figure 4. Functional enrichment analysis of the overlapping genes. (A) Filtering of the overlapping genes. (B) Gene Ontology functional enrichment analysis. (C) Kyoto Encyclopedia of Genes and Genomes pathway analysis of the enriched genes. GEO, Gene Expression Omnibus; TCGA, The Cancer Genome Atlas.

cDNA from 12 pairs of normal and cancer tissues were used in RT-qPCR, to verify the results of the bioinformatics analysis. As shown in Fig. 5E-G, only *SCGB1A1* expression changes were consistent with the bioinformatics analysis. The expression levels of *SCGB1A1* in normal tissues were significantly higher than in the cancer tissues. The trend in *SCGB1A1* expression was also confirmed using immunohistochemical staining (Fig. 5H and I). The viability of cancer cell lines stably overexpressing SCGB1A1 was lower than that of the control group cancer cells (Fig. 5J). Furthermore, pan-cancer analysis revealed that the expression levels of *SCGB1A1* in normal tissues were significantly higher than in tumor tissues (Fig. 5K). According to the expression characteristics, *SCGB1A1* may be used as a novel biomarker to improve the diagnosis of HNSCC.

Drug sensitivity and molecular docking analysis. To further explore the role of *SCGB1A1* in HNSCC therapy, two types of oral squamous cell carcinoma cell lines were used as *in vitro* models and treated with DOX, a chemotherapeutic agent primarily employed for the treatment of cancer, including HNSCC. The expression level of *SCGB1A1* was upregulated during DOX-induced tumor cell apoptosis (Fig. 6A-D). Therefore, *SCGB1A1* may serve as a biomarker for evaluating the effectiveness of cancer therapy.

In addition, the results of a drug sensitivity analysis indicated that the SCGB1A1 expression level in cancer cells exhibited a significant increase after DOX treatment (Figs. 6E, F and S6). Furthermore, certain drug molecules could bind directly to the SCGB1A1 protein, such as Tubastatin A and TG101348 (Fedratinib) (Fig. 6G and H), which may exert anticancer properties by regulating the SCGB1A1 protein. These data may explain why patients with upregulated expression of SCGB1A1 had a longer survival time. In summary, it was demonstrated that SCGB1A1 may serve as a candidate therapeutic target for the management of HNSCC.

Immunological function analysis of SCGB1A1. It is well-established that the immune microenvironment has a notable influence on the effectiveness of cancer treatment (55). Of note, the results of the present study showed that *SCGB1A1* expression was negatively correlated with immune adjustment by regulating the infiltration, activation and differentiation of immune cells, such as $CD8^+$ cells, $CD4^+$ cells, dendritic cells and macrophages (Fig. 7A). Furthermore, *SCGB1A1* expression was also correlated with immune checkpoint proteins, including CD274 and PDCD1LG2 (Fig. 7B). These results demonstrated that *SCGB1A1* may be a candidate therapeutic target for the management of HNSCC.

Regulatory mechanism analysis of SCGB1A1. Due to *SCGB1A1* exerting numerous functions in HSNCC therapy, the underlying mechanisms of *SCGB1A1* were further explored. Gene interaction networks were built to understand the functional biological mechanisms of *SCGB1A1* using GeneMANIA. A total of 20 genes associated with *SCGB1A1* were identified, and the results showed that these genes were involved in the 'Regulation of cell-cell adhesion mediated by cadherin', 'Intracellular steroid hormone receptor signaling pathway', 'Steroid hormone mediated signaling pathway', 'Cell-cell adhesion mediated by cadherin', 'Cellular response to steroid hormone stimulus' and 'Hormone-mediated signaling pathway' (Fig. 7C). To further elucidate the molecular mechanisms of *SCGB1A1* in HNSCC, GSEA was performed using TCGA RNA-seq data.

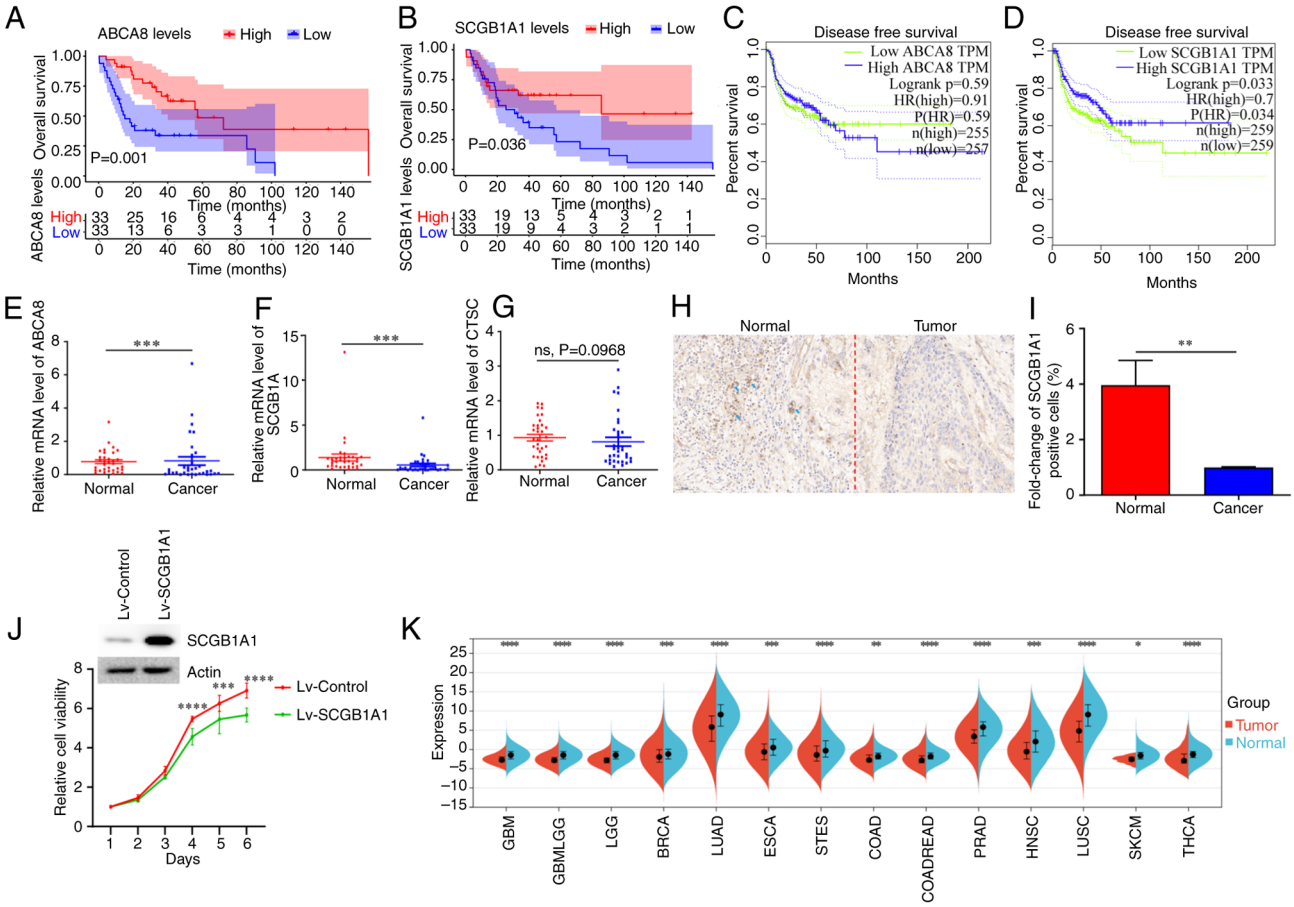

Figure 5. Survival analysis and expression characteristics of SCGB1A1. (A) Overall survival analysis of *ABCA8*. (B) Overall survival analysis of *SCGB1A1*. (C) Disease-free survival analysis of *ABCA8*. (D) Disease-free survival analysis of *SCGB1A1*. (E) *ABCA8*, (F) *SCGB1A1*, and (G) *CTSC* expression levels in the clinical samples. (H) Immunohistochemical staining of *SCGB1A1* in the clinical sample. Representative SCGB1A1$^+$ cells are marked with blue arrows. Scale bar, 50 μm. (I) Statistical analysis of SCGB1A1$^+$ cells after immunohistochemical staining. (J) The knockdown of SCGB1A1 expression following Lv-SCGB1A1 transduction. The viability of Lv-SCGB1A1-infected and Lv-Control-infected CAL27 cells were determined using a Cell Counting Kit-8 assay. (K) Analysis of *SCGB1A1* expression levels in the pan-cancerous tissue. **P<0.01, ***P<0.001, ****P<0.0001. ABCA8, ATP binding cassette subfamily A member 8; CTSC, cathepsin C; HR, hazard ratio; ns, not significant; Lv-SCGB1A1, lentiviral SCGB1A1; TPM, transcripts per million; SCGB1A1, secretoglobin family 1A member 1.

As shown in Fig. 7D, downregulated expression of *SCGB1A1* was associated with 'ECM RECEPTOR INTERACTION', 'ADIPOCYTOKINE SIGNALING PATHWAY', 'TGF BETA SIGNALING PATHWAY', 'PATHWAYS IN CANCER' and 'FOCAL ADHESION', which were highly associated with cancer cell proliferation, metabolism, immune escape and migration. As shown in Figs. 7E and S7, the mechanism of action of SCGB1A1 was primarily enriched for metabolism pathways when it was upregulated, such as 'GLYCOLYSIS GLUCONEOGENESIS', 'ASCORBATE AND ALDARATE METABOLISM', 'DRUG METABOLISM CYTOCHROME P450', 'STARCH AND SUCROSE METABOLISM', 'METABOLISM OF XENOBIOTICS BY CYTOCHROME P450', 'PENTOSE AND GLUCURONATE INTERCONVERSIONS', 'PORPHYRIN AND CHLOROPHYLL METABOLISM', 'TYROSINE METABOLISM', 'RETINOL METABOLISM' and 'ARACHIDONIC ACID METABOLISM'. Based on these findings, SCGB1A1 may be a potential target for HNSCC therapy.

Analysis of glycolytic genes. To understand the association between SCGB1A1 and the glycolytic pathway, 21 key glycolytic genes were obtained by intersecting the clustering differential genes obtained through previous clustering analysis with 200 glycolysis-related genes collected in the GSEA MSigDB gene sets (Fig. 8A). First, the mutations of 21 glycolysis-associated genes were examined and found that 18 genes, such as collagen type V α1 chain (*COL5A1*), *PHKA2*, *CHST6*, *MERTK*, *DSC2*, *PYGL*, *ABCB6*, *GPC3*, *IDUA*, *GCLC*, *BIK*, nuclear autoantigenic sperm protein *(NASP)*, *P4HA2*, *B4GALT4*, *CXCR4*, *ELF3*, *ENO2* and *NT5E*, exhibited varying degrees of mutations, with a maximum degree of mutation of 3% (Fig. 8B). Among them, three types of mutations were more common: Missense mutations, nonsense mutations and splice site. In addition, the coexistence and exclusion relationships of these 18 mutated glycolytic genes were also analyzed and it was found that *CXCR4* and *ABCB6*, and *B4GALT4* and *BIK* exhibited coexistence relationships (Fig. 8C).

Immunological characteristics and the relationship with prognosis of glycolytic genes. The immune characteristics of glycolysis-related genes were assessed to understand the relationship between glycolysis and tumor immune escape. First, a proportional risk regression model was used to classify genes for risk. Next, 79 immune checkpoint genes were

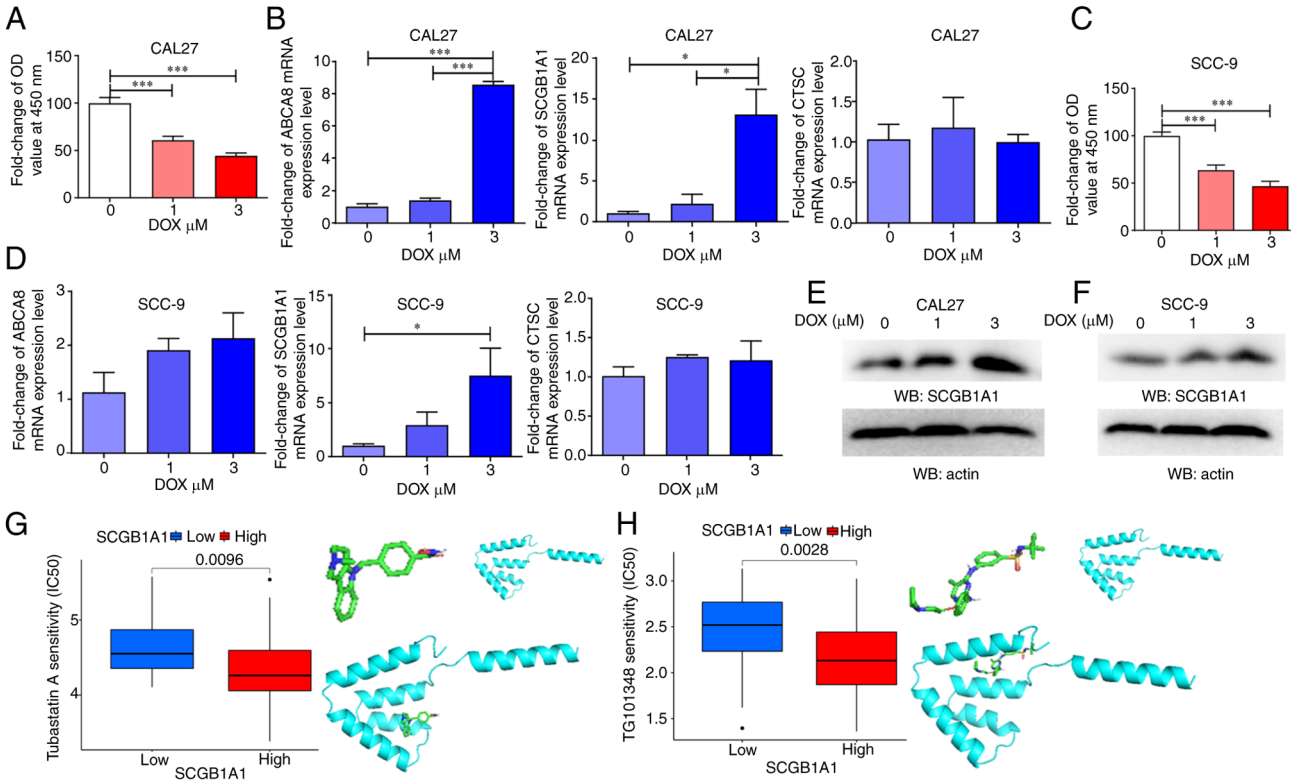

Figure 6. Drug sensitivity and molecular docking analysis. (A) CCK-8 assay to determine the viability of DOX-treated CAL27 cells. (B) The mRNA expression levels of hub genes in the DOX-treated CAL27 cells. (C) CCK-8 assay to determine the viability of DOX-treated SCC-9 cells. (D) The mRNA expression levels of hub genes in the DOX-treated SCC-9 cells. The expression level of SCGB1A1 protein induced by DOX in (E) CAL27 and (F) SCC-9 cells was assessed using western blotting. (G) Tubastatin A and (H) TG101348 sensitivity and molecular docking analysis of *SCGB1A1*. *P<0.05, ***P<0.001. CCK-8, Cell Counting Kit-8; DOX, doxorubicin; OD, optical density; ABCA8, ATP binding cassette subfamily A member 8; CTSC, cathepsin C; SCGB1A1, secretoglobin family 1A member 1.

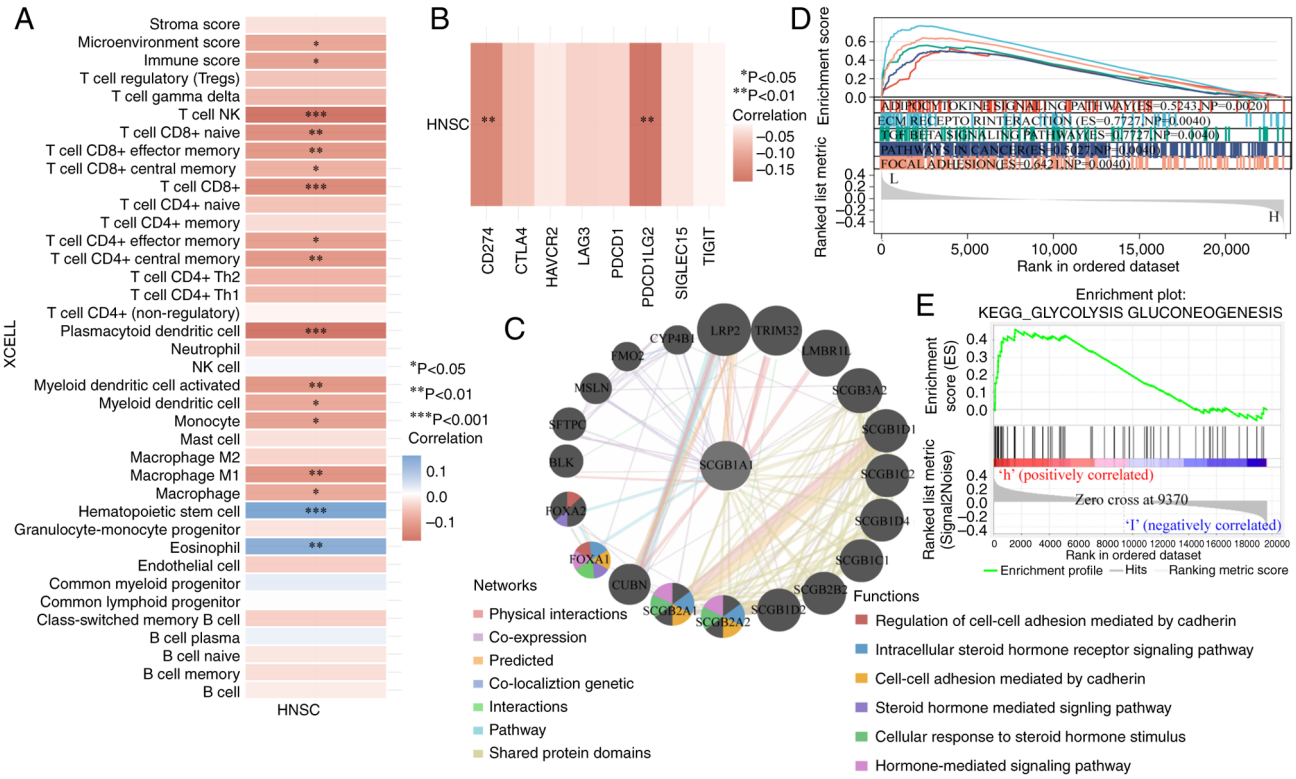

Figure 7. Immunological functional analysis of *SCGB1A1*. (A) Correlation analysis of *SCGB1A1* with immune characteristics. (B) Analysis of the correlation of SCGB1A1 with immune checkpoint proteins. (C) Protein-protein interaction networks of SCGB1A1. (D and E) Gene Set Enrichment Analysis of *SCGB1A1*. *P<0.05, **P<0.01 and ***P<0.001. HNSC, head and neck squamous cell carcinoma; KEGG, Kyoto Encyclopedia of Genes and Genomes; SCGB1A1, secretoglobin family 1A member 1.

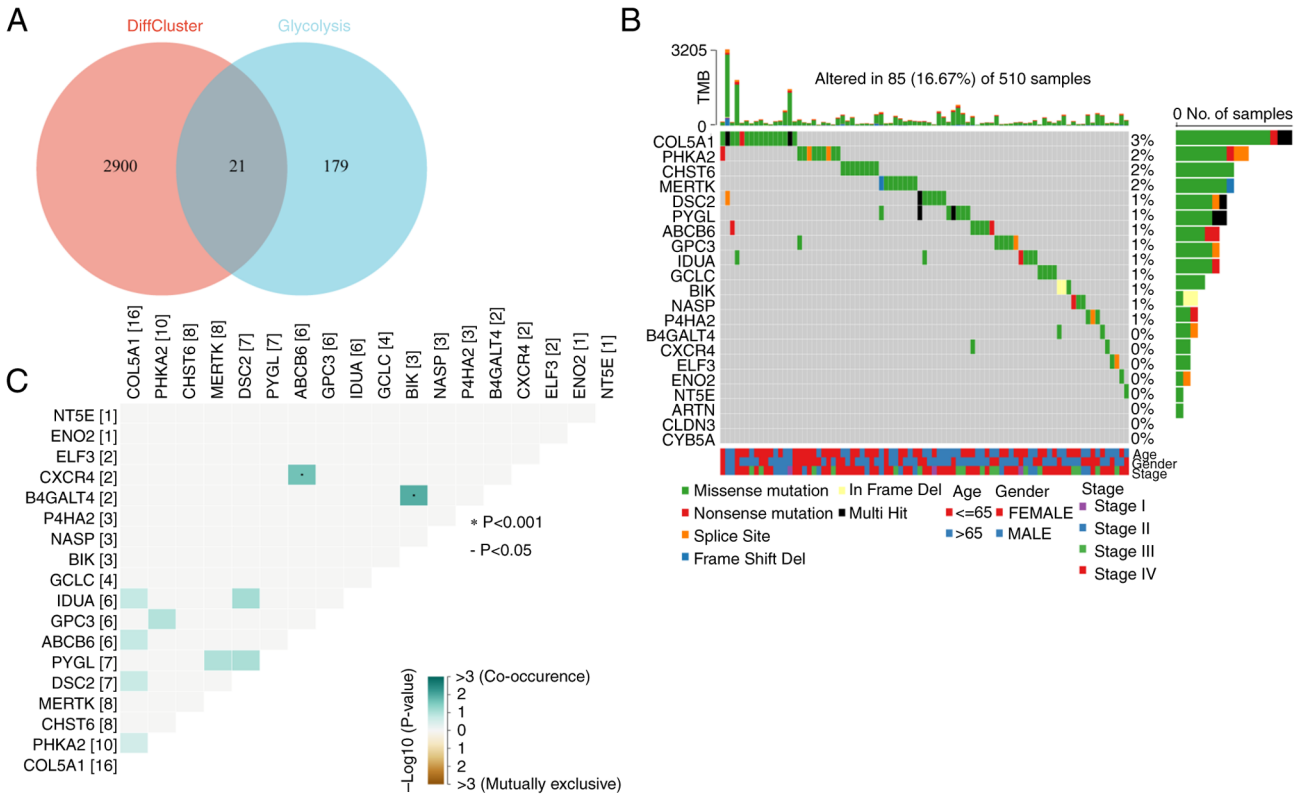

Figure 8. Mutational properties of glycolysis-related genes. (A) Venn diagram of glycolytic genes and unsupervised clustering analysis of the genes. (B) Mutation characteristics of the 21 genes in the TCGA-HNSC dataset. (C) Co-occurrence characteristics of the glycolytic genes in TCGA-HNSC. TCGA, The Cancer Genome Atlas; HNSC, head and neck squamous cell carcinoma.

collected (56) and the correlation heatmap with glycolysis genes was analyzed. It was found that *BIK*, *COL5A1* and *CYB5A* were negatively correlated with the majority of immune checkpoint genes, while *IDUA*, *MERTK* and *NASP* were positively correlated with the majority of immune checkpoint genes (Fig. 9A). In subsequent prognostic analysis, it was found that high expression of *COL5A1* was associated with a good prognosis, while downregulated expression of *NASP* was associated with a worse prognosis (Figs. 9B and S8). Subsequently, the correlation between immune cells and these 2 genes was analyzed, and it was found that *COL5A1* was significantly positively correlated with resting $CD4^+$ memory T cells and M0 macrophages, while it was significantly negatively correlated with T follicular helper cells and activated $CD4^+$ memory T cells (Fig. 9C). The *NASP* glycolytic gene was significantly positively correlated with T follicular helper cells and activated $CD4^+$ memory T cells (Fig. 9D), while it was significantly negatively correlated with M0 macrophages and other cells (Fig. S9). In recent years, emerging immunotherapies, including immune checkpoint inhibitors, have achieved notable results in clinical practice. To investigate the role of the glycolytic genes, *COL5A1* and *NASP*, in immunotherapy, patients were stratified based on their individual gene expression levels and it was observed that the *COL5A1* or *NASP* low expression groups exhibited significant therapeutic efficacy upon CTLA4 treatment (Fig. 9E and F). In the gene correlation analysis, it was found that *SCGB1A1* was positively correlated with *NASP* (Fig. 9G), while its correlation with other glycolytic genes was low (Fig. S10).

Discussion

HNSCC is one of the most common types of cancer and is associated with high morbidity and mortality rates (57,58). Exploring novel biomarkers and therapeutic targets for HNSCC may contribute to the diagnosis, prognostic evaluation and therapeutic management of HNSCC, and may also decrease the economic burden on patients and society.

SCGB1A1 is an important gene that is implicated in several pulmonary diseases, including asthma, chronic obstructive pulmonary disease and lung cancer (59). A study conducted by Xu *et al* (60) revealed the crucial role of SCGB1A1 in modulating alveolar macrophage-mediated inflammation and immune responses, as well as attenuating cytokine surges within the lungs. Yu *et al* (61) demonstrated that excessive expression of SCGB1A1 in the heart can result in the development of myocardial hypertrophy. Moreover, SCGB1A1 can inhibit the Th17 response by regulating dendritic cells in allergic rhinitis (62). Downregulation of *SCGB1A1* affects tumorigenicity in non-small cell lung cancer (63) and mouse lung cancer models (64). These studies therefore indicate a potential role for *SCGB1A1* in the development of numerous diseases. However, to the best of our knowledge, the roles of *SCGB1A1* in HNSCC have not been previously reported in the literature. In the present study, it was found that *SCGB1A1* may serve as a novel biomarker for the diagnostic and prognostic evaluation of HNSCC. Notably, the expression levels of *SCGB1A1* were significantly positively associated with patient outcomes.

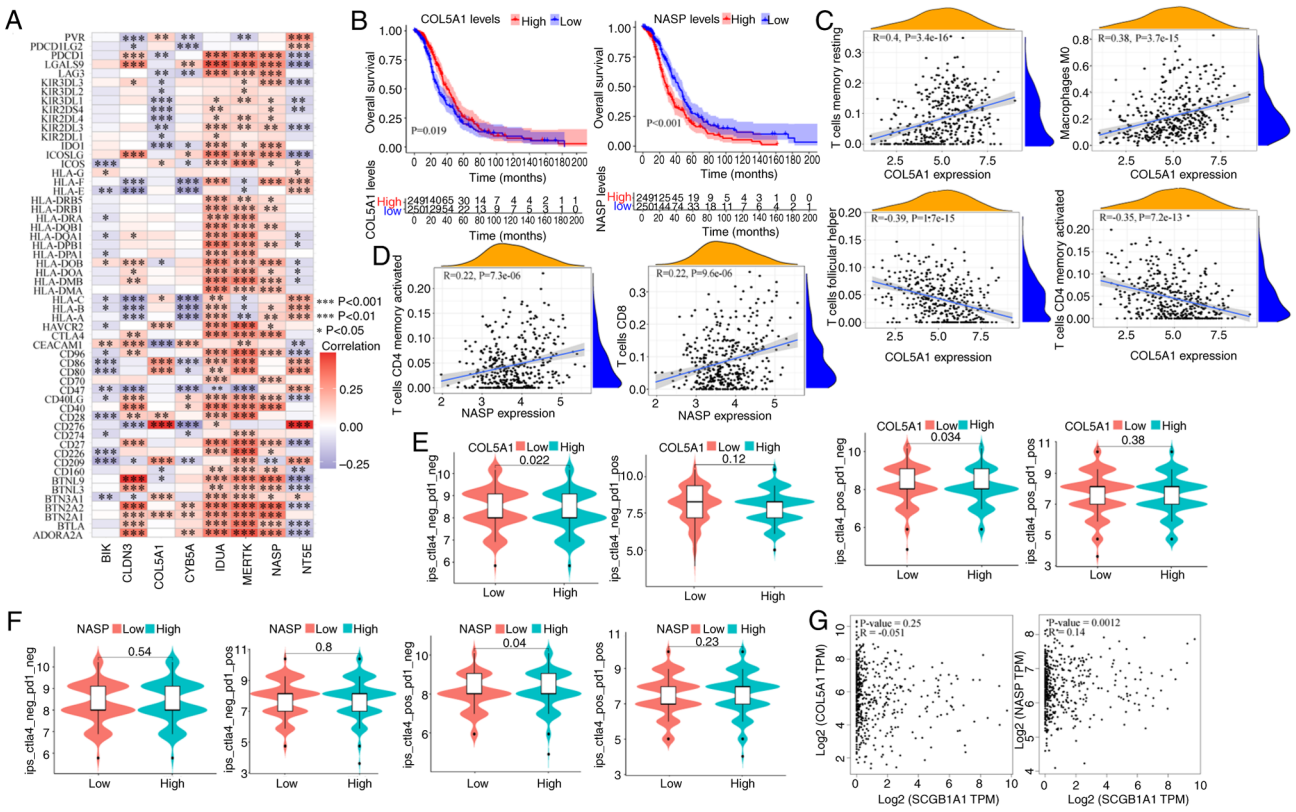

Figure 9. Immunological characteristics of glycolytic genes. (A) Heat map of the correlation between glycolytic genes and immune checkpoint genes. (B) Survival analysis of *COL5A1* and *NASP*. Correlation analysis between (C) *COL5A1* and (D) *NASP* with immune cells. Immunotherapy analysis of (E) *COL5A1* and (F) *NASP*. (G) Correlation analysis between secretoglobin family 1A member 1 and *COL5A1* or *NASP*. *P<0.05, **P<0.01 and ***P<0.001. COL5A1, collagen type V α1 chain; NASP, nuclear autoantigenic sperm protein; TPM, transcripts per million.

Additionally, SCGB1A1 may also serve as a potential therapeutic target for the management of HNSCC. The SCGB1A1 protein is 10 kDa, imbues acid, heat and protease resistance and can be produced in large quantities through recombinant protein expression. These characteristics of SCGB1A1 make it an ideal candidate for further comprehensive investigation, thereby augmenting the potential of targeted therapy with this protein (65). The present study revealed that the expression levels of *SCGB1A1* were strongly correlated with drug sensitivity and the immune microenvironment. Further exploration found that *SCGB1A1* was involved in several pathways that are significantly associated with several types of cancer. However, the predicted non-specific effect of targeting or administering SCGB1A1 may limit its clinical utilization. The delivery of SCGB1A1 into cancer cells using oncolytic viruses can potentially address this issue. Nevertheless, further verification is necessary to confirm the feasibility of this strategy.

Adipocytokines have been reported to impact cancer cell proliferation, invasion and migration directly. TGF-β is an immune-suppressive cytokine that restricts the activity of effector immune cells, which can result in tumor development by generating and maintaining a highly immune-suppressive tumor environment (66). Focal adhesion molecules play a key role in allowing cells to attach to the extracellular matrix and mediate numerous biological functions. Reduced expression of focal adhesion molecules has been associated with enhanced cell migration and cancer metastasis (67). In addition, the results of the present study demonstrated that the expression level of *SCGB1A1* was highly correlated with glycolytic enzymes, which may confer heightened susceptibility of tumor cells to cytotoxic T lymphocytes and initiate innate immune responses (68,69). Moreover, the immune checkpoint molecules associated with *SCGB1A1* exhibit promising antitumor activity in the clinical treatment of patients with HNSCC (70). Therefore, SCGB1A1 may serve as an attractive therapeutic target for the management of cancer due to its multiple regulatory functions.

In the present study, a relatively limited number of clinical samples were obtained to validate the accuracy of the bioinformatics analyses. In future, the sample size will be expanded in further research endeavors to further substantiate the precision of the bioinformatics analysis results and to investigate the underlying mechanism of action of SCGB1A1. In conclusion, the biomarker, *SCGB1A1*, exhibits versatility in its application for the diagnosis, evaluation of treatment response, immune assessment and prognosis evaluation of HNSCC. Furthermore, SCGB1A1 demonstrates potential as a promising therapeutic target.

Acknowledgements

Not applicable.

Funding

The present study was supported by The Natural Science Foundation of Shandong (grant no. ZR2020QH160),

New Industry Cultivation Program of Qingdao (grant no. 23-1-4-xxgg-18-nsh) and Technological SMEs Innovation Ability Improvement Project of Shandong Province (grant no. 2023TSGC0510).

Availability of data and materials

The data generated in the present study may be requested from the corresponding author.

Authors' contributions

Project administration was conducted by JW, QX and ZY. JW, QX, RY and ZY contributed to conception and design. Experiments and data analysis were conducted by JW, QX, LY, JY, ZC and YC. JW, QX and AX also contributed to the acquisition of data. Original manuscript draft preparation was conducted by JW, QX, LY and AX. Reviewing and editing of the manuscript was conducted by RY and ZY. All authors read and approved the final version of the manuscript. JW, QX, RY and ZY confirm the authenticity of all the raw data.

Ethics approval and consent to participate

The clinical sample collection was performed according to the protocols approved by the Ethics Committee of the Medical College of Qingdao University (Qingdao, China; QDU-HEC-2022166). All patients provided written consented for participation in the present study.

Patient consent for publication

The patients provided consent for their information to be published.

Competing interests

The authors declare that they have no competing interests.

References

1. Raj S, Kesari KK, Kumar A, Rathi B, Sharma A, Gupta PK, Jha SK, Jha NK, Slama P, Roychoudhury S and Kumar D: Molecular mechanism(s) of regulation(s) of c-MET/HGF signaling in head and neck cancer. Mol Cancer 21: 31, 2022.
2. Tang E, Lahmi L, Meillan N, Pietta G, Albert S and Maingon P: Treatment strategy for distant synchronous metastatic head and neck squamous cell carcinoma. Curr Oncol Rep 21: 102, 2019.
3. Chow LQM: Head and neck cancer. N Engl J Med 382: 60-72, 2020.
4. Bray F, Ferlay J, Soerjomataram I, Siegel RL, Torre LA and Jemal A: Global cancer statistics 2018: GLOBOCAN estimates of incidence and mortality worldwide for 36 cancers in 185 countries. CA Cancer J Clin 68: 394-424, 2018.
5. Vahabi M, Blandino G and Di Agostino S: MicroRNAs in head and neck squamous cell carcinoma: A possible challenge as biomarkers, determinants for the choice of therapy and targets for personalized molecular therapies. Transl Cancer Res 10: 3090-3110, 2021.
6. Global Burden of Disease Cancer Collaboration; Fitzmaurice C, Allen C, Barber RM, Barregard L, Bhutta ZA, Brenner H, Dicker DJ, Chimed-Orchir O, Dandona R, *et al*: Global, regional, and national cancer incidence, mortality, years of life lost, years lived with disability, and disability-adjusted life-years for 32 cancer groups, 1990 to 2015: A systematic analysis for the global burden of disease study. JAMA Oncol 3: 524-548, 2017.
7. Hakim M, Billan S, Tisch U, Peng G, Dvrokind I, Marom O, Abdah-Bortnyak R, Kuten A and Haick H: Diagnosis of head-and-neck cancer from exhaled breath. Br J Cancer 104: 1649-1655, 2011.
8. Schötz U, Balzer V, Brandt FW, Ziemann F, Subtil FSB, Rieckmann T, Köcher S, Engenhart-Cabillic R, Dikomey E, Wittig A and Arenz A: Dual PI3K/mTOR inhibitor NVP-BEZ235 enhances radiosensitivity of head and neck squamous cell carcinoma (HNSCC) cell lines due to suppressed double-strand break (DSB) repair by non-homologous end joining. Cancers (Basel) 12: 467, 2020.
9. You Y, Tian Z, Du Z, Wu K, Xu G, Dai M, Wang Y and Xiao M: M1-like tumor-associated macrophages cascade a mesenchymal/stem-like phenotype of oral squamous cell carcinoma via the IL6/Stat3/THBS1 feedback loop. J Exp Clin Cancer Res 41: 10, 2022.
10. Tokheim CJ, Papadopoulos N, Kinzler KW, Vogelstein B and Karchin R: Evaluating the evaluation of cancer driver genes. Proc Natl Acad Sci USA 113: 14330, 2016.
11. Andrea S, Paola M, Claudio P, Urbani G, Allegretti M, Pellini R, Mehterov N, Ben-David U, Strano S, Bossi P and Blandino G: Immunosignatures associated with TP53 status and co-mutations classify prognostically head and neck cancer patients. Mol Cancer 22: 192, 2023.
12. Kong W, Han Y, Gu H, Yang H and Zang Y: TP53 mutation-associated immune infiltration and a novel risk score model in HNSCC. Biochem Biophys Rep 32: 101359, 2022.
13. El Baroudi M, Machiels JP and Schmitz S: Expression of SESN1, UHRF1BP1, and miR-377-3p as prognostic markers in mutated TP53 squamous cell carcinoma of the head and neck. Cancer Biol Ther 18: 775-782, 2017.
14. Wei Z, Shen Y, Zhou C, Cao Y, Deng H and Shen Z: CD3D: A prognostic biomarker associated with immune infiltration and immunotherapeutic response in head and neck squamous cell carcinoma. Bioengineered 13: 13784-13800, 2022.
15. Chen Y, Yang J, Jin H, Wen W, Xu Y, Zhang X and Wang Y: HtrA3: A promising prognostic biomarker and therapeutic target for head and neck squamous cell carcinoma. PeerJ 11: e16237, 2023.
16. Chen C, Méndez E, Houck J, Fan W, Lohavanichbutr P, Doody D, Yueh B, Futran ND, Upton M, Farwell DG, *et al*: Gene expression profiling identifies genes predictive of oral squamous cell carcinoma. Cancer Epidemiol Biomarkers Prev 17: 2152-2162, 2008.
17. Zhang Y, Luo S, Jia Y and Zhang X: Telomere maintenance mechanism dysregulation serves as an early predictor of adjuvant therapy response and a potential therapeutic target in human cancers. Int J Cancer 151: 313-327, 2022.
18. Leemans CR, Snijders PJF and Brakenhoff RH: The molecular landscape of head and neck cancer. Nat Rev Cancer 18: 269-282, 2018.
19. Han D, Yu Z, Zhang H, Liu H, Wang B and Qian D: Microenvironment-associated gene HSD11B1 may serve as a prognostic biomarker in clear cell renal cell carcinoma: A study based on TCGA, RT-qPCR, Western blotting, and immunohistochemistry. Bioengineered 12: 10891-10904, 2021.
20. Ritchie ME, Phipson B, Wu D, Hu Y, Law CW, Shi W and Smyth GK: limma powers differential expression analyses for RNA-sequencing and microarray studies. Nucleic Acids Res 43: e47, 2015.
21. RStudio Team: RStudio: Integrated Development for R. RStudio, Inc., Boston, MA, 2015.
22. Shippy DC and Ulland TK: Lipid metabolism transcriptomics of murine microglia in Alzheimer's disease and neuroinflammation. Sci Rep 13: 14800, 2023.
23. Luo L, Zhu J, Guo Y and Li C: Mitophagy and immune infiltration in vitiligo: Evidence from bioinformatics analysis. Front Immunol 14: 1164124, 2023.
24. Langfelder P and Horvath S: WGCNA: An R package for weighted correlation network analysis. BMC Bioinformatics 9: 559, 2008.
25. Liu B, Ma X and Ha W: Identification of potential prognostic biomarkers associated with macrophage M2 infiltration in gastric cancer. Front Genet 12: 827444, 2022.
26. Pei G, Chen L and Zhang W: WGCNA application to proteomic and metabolomic data analysis. Methods Enzymol 585: 135-158, 2017.
27. Wilkerson MD and Hayes DN: ConsensusClusterPlus: A class discovery tool with confidence assessments and item tracking. Bioinformatics 26: 1572-1573, 2010.

28. Gao CH, Yu G and Cai P: ggVennDiagram: An intuitive, easy-to-use, and highly customizable r package to generate venn diagram. Front Genet 12: 706907, 2021.
29. Thomas PD: The gene ontology and the meaning of biological function. Methods Mol Biol 1446: 15-24, 2017.
30. Kanehisa M, Furumichi M, Tanabe M, Sato Y and Morishima K: KEGG: New perspectives on genomes, pathways, diseases and drugs. Nucleic Acids Res 45: D353-D361, 2017.
31. Liberzon A, Birger C, Thorvaldsdóttir H, Ghandi M, Mesirov JP and Tamayo P: The molecular signatures database (MSigDB) hallmark gene set collection. Cell Syst 1: 417-425, 2015.
32. Szklarczyk D, Gable AL, Lyon D, Junge A, Wyder S, Huerta-Cepas J, Simonovic M, Doncheva NT, Morris JH, Bork P, *et al*: STRING v11: Protein-protein association networks with increased coverage, supporting functional discovery in genome-wide experimental datasets. Nucleic Acids Res 47: D607-D613, 2019.
33. Shannon P, Markiel A, Ozier O, Baliga NS, Wang JT, Ramage D, Amin N, Schwikowski B and Ideker T: Cytoscape: A software environment for integrated models of biomolecular interaction networks. Genome Res 13: 2498-2504, 2003.
34. Chin CH, Chen SH, Wu HH, Ho CW, Ko MT and Lin CY: cytoHubba: Identifying hub objects and sub-networks from complex interactome. BMC Syst Biol 8 (Suppl 4): S11, 2014.
35. Hess AS and Hess JR: Kaplan-Meier survival curves. Transfusion 60: 670-672, 2020.
36. Goel MK, Khanna P and Kishore J: Understanding survival analysis: Kaplan-Meier estimate. Int J Ayurveda Res 1: 274-278, 2010.
37. Mu H, Wang Z, Zhang X, Qian D, Wang Y, Jiang S, Liang S and Wang B: HCMV-encoded IE2 induces anxiety-depression and cognitive impairment in UL122 genetically-modified mice. Int J Clin Exp Pathol 12: 4087-4095, 2019.
38. Livak KJ and Schmittgen TD: Analysis of relative gene expression data using real-time quantitative PCR and the 2(-Delta Delta C(T)) method. Methods 25: 402-408, 2001.
39. Geeleher P, Cox N and Huang RS: pRRophetic: An R package for prediction of clinical chemotherapeutic response from tumor gene expression levels. PLoS One 9: e107468, 2014.
40. Geeleher P, Cox NJ and Huang RS: Clinical drug response can be predicted using baseline gene expression levels and in vitro drug sensitivity in cell lines. Genome Biol 15: R47, 2014.
41. El-Hachem N, Haibe-Kains B, Khalil A, Kobeissy FH and Nemer G: AutoDock and AutoDockTools for protein-ligand docking: Beta-site amyloid precursor protein cleaving enzyme 1(BACE1) as a case study. Methods Mol Biol 1598: 391-403, 2017.
42. Sugano-Nakamura N, Matoba K, Hirose M, Bashiruddin NK, Matsunaga Y, Yamashita K, Hirata K, Yamamoto M, Arimori T, Suga H and Takagi J: De novo Fc-based receptor dimerizers differentially modulate PlexinB1 function. Structure 30: 1411-1423.e4, 2022.
43. Tao Q, Du J, Li X, Zeng J, Tan B, Xu J, Lin W and Chen XL: Network pharmacology and molecular docking analysis on molecular targets and mechanisms of Huashi Baidu formula in the treatment of COVID-19. Drug Dev Ind Pharm 46: 1345-1353, 2020.
44. Zeng D, Li M, Zhou R, Zhang J, Sun H, Shi M, Bin J, Liao Y, Rao J and Liao W: Tumor microenvironment characterization in gastric cancer identifies prognostic and immunotherapeutically relevant gene signatures. Cancer Immunol Res 7: 737-750, 2019.
45. Sturm G, Finotello F, Petitprez F, Zhang JD, Baumbach J, Fridman WH, List M and Aneichyk T: Comprehensive evaluation of transcriptome-based cell-type quantification methods for immuno-oncology. Bioinformatics 35: i436-i445, 2019.
46. Li B, Severson E, Pignon JC, Zhao H, Li T, Novak J, Jiang P, Shen H, Aster JC, Rodig S, *et al*: Comprehensive analyses of tumor immunity: Implications for cancer immunotherapy. Genome Biol 17: 174, 2016.
47. Aran D, Hu Z and Butte AJ: xCell: Digitally portraying the tissue cellular heterogeneity landscape. Genome Biol 18: 220, 2017.
48. Li T, Fu J, Zeng Z, Cohen D, Li J, Chen Q, Li B and Liu XS: TIMER2.0 for analysis of tumor-infiltrating immune cells. Nucleic Acids Res 48: W509-W514, 2020.
49. Wang J, Sun J, Liu LN, Flies DB, Nie X, Toki M, Zhang J, Song C, Zarr M, Zhou X, *et al*: Siglec-15 as an immune suppressor and potential target for normalization cancer immunotherapy. Nat Med 25: 656-666, 2019.
50. Frost FG, Cherukuri PF, Milanovich S and Boerkoel CF: Pan-cancer RNA-seq data stratifies tumours by some hallmarks of cancer. J Cell Mol Med 24: 418-430, 2020.
51. Izzi V, Davis MN and Naba A: Pan-cancer analysis of the genomic alterations and mutations of the matrisome. Cancers (Basel) 12: 2046, 2020.
52. Zhang Q, Huang R, Hu H, Yu L, Tang Q, Tao Y, Liu Z, Li J and Wang G: Integrative analysis of hypoxia-associated signature in pan-cancer. iScience 23: 101460, 2020.
53. Franz M, Rodriguez H, Lopes C, Zuberi K, Montojo J, Bader GD and Morris Q: GeneMANIA update 2018. Nucleic Acids Res 46: W60-W64, 2018.
54. Mayakonda A, Lin DC, Assenov Y, Plass C and Koeffler HP: Maftools: Efficient and comprehensive analysis of somatic variants in cancer. Genome Res 28: 1747-1756, 2018.
55. Jiang L and Liu J: Immunological effect of tyrosine kinase inhibitors on the tumor immune environment in non-small cell lung cancer. Oncol Lett 23: 165, 2022.
56. Hu FF, Liu CJ, Liu LL, Zhang Q and Guo AY: Expression profile of immune checkpoint genes and their roles in predicting immunotherapy response. Brief Bioinform 22: bbaa176, 2021.
57. Barsouk A, Aluru JS, Rawla P, Saginala K and Barsouk A: Epidemiology, risk factors, and prevention of head and neck squamous cell carcinoma. Med Sci (Basel) 11: 42, 2023.
58. Trivedi S, Sun L and Aggarwal C: Immunotherapy for head and neck cancer. Hematol Oncol Clin North Am 35: 1021-1037, 2021.
59. Li XX, Peng T, Gao J, Feng JG, Wu DD, Yang T, Zhong L, Fu WP and Sun C: Allele-specific expression identified rs2509956 as a novel long-distance cis-regulatory SNP for SCGB1A1, an important gene for multiple pulmonary diseases. Am J Physiol Lung Cell Mol Physiol 317: L456-L463, 2019.
60. Xu M, Yang W, Wang X and Nayak DK: Lung secretoglobin Scgb1a1 influences alveolar macrophage-mediated inflammation and immunity. Front Immunol 11: 584310, 2020.
61. Yu Y, Liu JY, Yang HJ, Luo XQ, Gao XP, Huang XX, Tang AX, Mary Cheng HY, Liu WC and Zhang P: Circadian disruption during fetal development promotes pathological cardiac remodeling in male mice. iScience 27: 109008, 2024.
62. Liu Y, Yu HJ, Wang N, Zhang YN, Huang SK, Cui YH and Liu Z: Clara cell 10-kDa protein inhibits T(H)17 responses through modulating dendritic cells in the setting of allergic rhinitis. J Allergy Clin Immunol 131: 387-394.e1-12, 2013.
63. Linnoila RI, Szabo E, DeMayo F, Witschi H, Sabourin C and Malkinson A: The role of CC10 in pulmonary carcinogenesis: From a marker to tumor suppression. Ann N Y Acad Sci 923: 249-267, 2000.
64. Hicks SM, Vassallo JD, Dieter MZ, Lewis CL, Whiteley LO, Fix AS and Lehman-McKeeman LD: Immunohistochemical analysis of Clara cell secretory protein expression in a transgenic model of mouse lung carcinogenesis. Toxicology 187: 217-228, 2003.
65. Pilon AL: Rationale for the development of recombinant human CC10 as a therapeutic for inflammatory and fibrotic disease. Ann N Y Acad Sci 923: 280-299, 2000.
66. Mirlekar B: Tumor promoting roles of IL-10, TGF-β, IL-4, and IL-35: Its implications in cancer immunotherapy. SAGE Open Med 10: 20503121211069012, 2022.
67. Lu J, Linares B, Xu Z and Rui YN: Mechanisms of FA-phagy, a new form of selective autophagy/organellophagy. Front Cell Dev Biol 9: 799123, 2021.
68. Wu L, Jin Y, Zhao X, Tang K, Zhao Y, Tong L, Yu X, Xiong K, Luo C, Zhu J, *et al*: Tumor aerobic glycolysis confers immune evasion through modulating sensitivity to T cell-mediated bystander killing via TNF-α. Cell Metab 35: 1580-1596.e9, 2023.
69. Yang FM, Chang HM and Yeh ETH: Regulation of TLR4 signaling through the TRAF6/sNASP axis by reversible phosphorylation mediated by CK2 and PP4. Proc Natl Acad Sci USA 118: e2107044118, 2021.
70. Economopoulou P, Agelaki S, Perisanidis C, Giotakis EI and Psyrri A: The promise of immunotherapy in head and neck squamous cell carcinoma. Ann Oncol 27: 1675-1685, 2016.